# Spatial reconstruction from contact networks: A unified approach for dynamics and genomics

Annick Lesne, Julien Mozziconnacci, Sofiane Ramdani

In 'Recurrence Plots and Their Quantifications: Methodological Breakthroughs and Interdisciplinary Discoveries'. Springer Proceedings in Complexity, 2024 (in press)

# Spatial reconstruction from contact networks: A unified approach for dynamics and genomics

Annick Lesne[1,2], Julien Mozziconacci[3,1], and Sofiane Ramdani[4]

[1] Sorbonne Université, CNRS, Laboratoire de Physique Théorique de la Matière Condensée, LPTMC, F-75252 Paris, France,
annick.lesne@cnrs.fr,
[2] Institut de Génétique Moléculaire de Montpellier, University of Montpellier, CNRS, F-34293 Montpellier, France,
[3] Muséum National d'Histoire Naturelle, Structure et Instabilité des Génomes, F-75231 Paris Cedex 5,
julien.mozziconacci@mnhn.fr,
[4] LIRMM, University of Montpellier, CNRS, Montpellier, France,
sofiane.ramdani@umontpellier.fr

**Abstract.** The physical proximity of genomic sites to each other, within the 3D structure of a chromosome, can be experimentally measured in living cells and represented in the form of a matrix, called a *contact map*. These maps are very similar to recurrence plots of dynamical systems. Consequently, the same methods can be used for reconstructing the underlying spatial structure, either the chromosome 3D spatial structure or the attractor in the phase space. These methods involve two steps: (1) deriving a complete distance matrix of the structure using graph distances on a contact network associated with the contact map; (2) reconstructing the structure from this distance matrix, using well-established methods from distance geometry or multidimensional scaling. We here review the different options for implementing the first step, according to the binary, graded or weighted nature of the contact map. We illustrate on three benchmarks (Lorenz model, white noise and EEG data) a novel spectral criterion reflecting the spatial dimension relevant in the second step.

**Keywords:** High-throughput chromosome conformation capture (Hi-C); Gram matrix; Graph distance; Distance geometry; Multidimensional scaling (MDS); Recurrence plot (RP); Spectral analysis.

## 1 Introduction

As seen from the other contributions in this volume, recurrence plots are an ubiquitous tool for quantitative analysis of time series. Starting from a time recording $(x_t)_t$, the methodology is to first derive $m$-dimensional delay vectors $X_t^{m,\tau} = [x_t, x_{t-\tau}, \ldots, x_{t-(m-1)\tau}]$ where $m$ is called the embedding dimension and $\tau$ is a tunable time delay [8, 20]. The Euclidean distances between each pair of delay vectors yield a square distance matrix, termed an *unthresholded recurrence plot*. A binary recurrence plot (RP) is obtained by replacing with 1

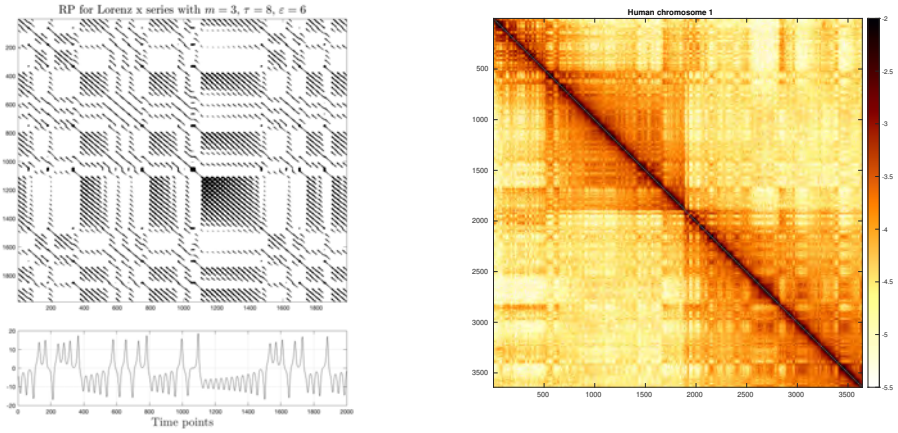


**Fig. 1. Recurrence plots and contact maps.** (Left) Recurrence plot of the $x$-component of the Lorenz attractor, drawn from a simulated trajectory (below, standard parameters $\sigma = 10$ , $r = 28$ and $b = 8/3$, $N = 2000$ time points) using the RP toolbox developed by N. Marwan [18] with an embedding dimension $m = 3$, a time delay $\tau = 8$ and a threshold $\epsilon = 6$. (Right) High-throughput contact map (Hi-C map) of human chromosome 1 in B-lymphoblastoid GM12878 cells, experimental data from [25], representing the frequency of pairwise spatial contacts between chromosomal sites, with color-coded contact frequency values ($\log_{10}$-scale color bar on the right side). For a clearer analogy, the origin has been located top left, as in a matrix, for both the recurrence plot and the Hi-C map.

the components smaller than a given radius $\epsilon$, and the larger ones with 0. Such a construction accommodates both time-continuous or time-discrete dynamics, and both continuous-valued or symbolic signals [9]. An ever-increasing number of methods and measures, gathered in the toolbox of *recurrence quantification analysis*, known as RQA, have been developed for extracting knowledge about the underlying dynamics directly from the RP [18, 19, 31].

The notion of recurrence, corresponding to pairs of points sufficiently close in the $m$-dimensional embedding phase space, can be straightforwardly extended from time series and trajectories of dynamical systems, to spatial conformations of linear polymer chains such as DNA and proteins. The time variable is replaced with the linear coordinate along the polymer, and phase space with real space.

Based on this analogy, application of recurrence quantification analysis to proteins offers a novel way to identify their local secondary structures from X-ray-resolved molecular structures, using the range of Van der Waals forces between amino-acids as a natural radius in constructing the recurrence plot [30]. As an exemple, diagonal lines in the contact map correspond to secondary structures known as $\alpha$ helices, while lines orthogonal to the main diagonal reflect the presence of other typical secondary structures termed $\beta$ sheets. In this context, protein contact networks are the counterpart of recurrence networks [6].

The situation for chromosomes is different, as contact maps are the only piece of high-throughput structural information experimentally accessible. Indeed, the scale of the chromosomes prevents a direct imaging of their 3D structure, and approaches based on the observation of fluorescent tags provide only low-resolution information about a limited number of sites. The development of chromosome conformation capture techniques [5] up to their high-throughput high-resolution whole-genome versions (Hi-C) has initiated a wide range of research about the biological functions of the chromosome spatial structure. The core technique involves a chemical crosslinking of close genome sites, digestion of the crosslinked pairs, re-ligation of the cross-linked fragments, and sequencing in order to identify pairs of genomic sites that were originally in close 3D proximity in the living cells. When the experimental process is performed on a population of cells, the result is a matrix of contact frequencies, known as a *Hi-C map*. Nowadays, it becomes possible to carry out the experiment in single cells, in which case the result is a binary presence/absence matrix (highly variable from cell to cell) [13]. In both cases, the analogy with recurrence plots is obvious (see Fig. 1), where the cross-linking range in 3D space (tuned by the concentration of cross-linking agent and the duration of its action) corresponds to the recurrence radius $\epsilon$. Chromosomal recurrences thus correspond to an experimentally determined proximity of genomic sites in 3D space (not to be confused with the recurrence of the A, T, G or C nucleotides along the 1D genomic sequence).

Reconstructing the spatial structure from a contact map could thus provide a visualization of an otherwise out-of-reach object. Another general outcome of the reconstruction is to assess the preservation of information when passing from a structure to a contact map, or from a signal to a recurrence plot [21, 29]. We will here review and revisit this dual issue, and present the benefits of combining methods developed for chaotic attractors and 3D chromosome structure.

## 2 Reconstructing a structure from a distance matrix

### 2.1 Using Gram matrices

A mathematically well-posed problem, solved long ago, is the reconstruction of a global structure from the knowledge of all pairwise distances $D_{ij}$ between its $N$ points. This domain is known a *distance geometry*. The first operation is to express the distance $D_{0i}$ between the barycenter $O$ and the point $P_i$, for any $i = 1, \ldots, N$, as a function of the elements of the distance matrix $D$:

$$D_{0i}^2 = \frac{1}{N}\sum_{j=1}^{N} D_{ij}^2 - \frac{1}{N^2}\sum_{j=1}^{N}\sum_{k>j}^{N} D_{jk}^2 \tag{1}$$

An auxiliary $N \times N$ matrix, the metric matrix $M$, is then constructed with elements:

$$M_{ij} = \frac{1}{2}\left[D_{0i}^2 + D_{0j}^2 - D_{ij}^2\right] \tag{2}$$

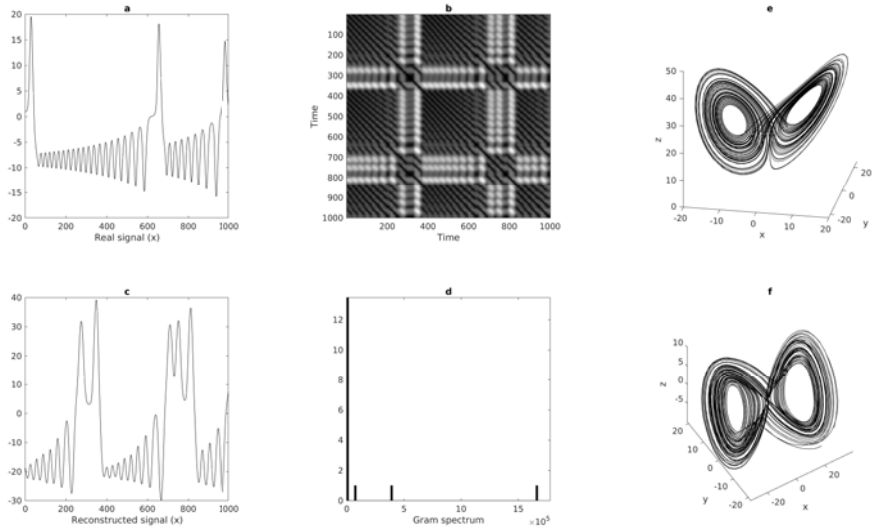


**Fig. 2. Reconstruction of Lorenz attractor from unthresholded RP using distance geometry.** (a) $x$-component of the simulated Lorenz dynamics ($N = 1000$ time points). (b) Corresponding unthresholded RP (i.e. Euclidean distance matrix), with embedding dimension $m = 8$ and time delay $\tau = 3$. Darker pixels correspond to smaller distances. (c) Principal eigenvector and (d) spectrum of the Gram matrix computed from the Euclidean distance matrix. Note the three markedly positive eigenvalues. (e) Original Lorenz attractor, simulated with $N = 3600$ time points after discarding the initial 700 steps (parameters $\sigma = 10$ , $r = 28$ and $b = 8/3$ with the notations of the original paper [17]). (f) Attractor reconstructed using distance geometry.

In the case of a single noiseless structure in an Euclidean space of dimension $d$, a theorem [10] states that the metric matrix $M$ has a rank $d$ and coincides with the Gram matrix $G$ of the $N$-point structure, whose element $G_{ij}$ is defined as the inner product between the vectors $OP_i$ and $OP_j$.

The central theorem of distance geometry [10] shows that, provided the Gram matrix $G$ is positive semi-definite, the coordinates of the points $P_i$ $(i = 1, \ldots, N)$ in the $d$-dimensional Euclidean space can be recovered from the $d$ first eigenvectors $V_a$ $(a = 1, \ldots, d)$ of the Gram matrix, normalized to 1 then rescaled by the square root of their associated eigenvalue $\lambda_a$, namely:

$$P_i(a) = V_a(i) \times \sqrt{\lambda_a} \quad \text{with} \quad \sum_{i=1}^{N} V_a(i)^2 = 1 \tag{3}$$

where $V_a(i)$ is the $i$-th component of the $N$-dimensional eigenvector $V_a$ and $P_i(a)$ is the $a$-coordinate of the point $P_i$. A key point of this theorem is the result that the rank $d$ of the Gram matrix $G$ determines the minimum dimension

$d$ of an embedding Euclidean space (not to be confused with the embedding dimension $m$ involved in the definition of recurrence plots or in Takens' theorem). Geometrically, the $d$ first eigenvectors of $G$ are the principal axes of the $N$-point structure, and the eigenvalues are the corresponding moments. The structure is reconstructed up to an isometry (e.g. rotation or dilation).

This geometrical reconstruction has been successfully applied to unthresholded RP [21, 26, 29]. We illustrate this approach for Lorenz attractor in Fig. 2. In the context of genomics, it is a basic ingredient of ShRec3D algorithm for reconstructing a consensus 3D structure from chrosomosomal contact maps and visualizing the average 3D shape of a chromosome ([4, 16] and figures therein).

### 2.2 Using multidimensional scaling (MDS)

In most practical situations, data are noisy and may come from the recording of several superimposed structures (several trajectories for a dynamical system, chromosomes of many cells for chromosome contact maps). As a signature of such a situation, the spectrum of the reconstructed Gram matrix $G$ displays more than $d$ non-vanishing eigenvalues, and even negative ones. Several statistical methods, introduced in various fields such as taxonomy [27], ecology [2] or psychological science [15] and now grouped under the name of *multidimensional scaling* (MDS), have been developed to derive the optimally matching structure, best corresponding to the available distance matrix affected by uncertainties. Several variants of MDS are besides possible (e.g. classical or metric) according to the optimization criteria chosen [4, 11, 23], and currently available in libraries.

Using MDS requires to know the dimension $d$ of the Euclidean space, in order to reconstruct the structure and not a projected version (supervised methodology). As evidenced in [16], a useful guideline is the presence of $d$ markedly positive eigenvalues in the spectrum of the Gram matrix $G$. However, in the case of chromosomes, the spatial dimension $d = 3$ is expected; the spectral gap between 3 positive eigenvalues and a cluster around 0 then shows the relevance of reconstructing a 3D consensus structure.

## 3 Reconstructing a distance matrix from a contact map

Starting from a contact map, the remaining issue for reconstructing the underlying structure is to determine a complete distance matrix, that is, a distance matrix with no undefined or infinite elements. The basic idea is to consider the contact map as the adjacency matrix of a network: the corresponding *contact network* [23]. This relationship between contact maps and contact networks has been successfully exploited with recurrence plots and the associated recurrence networks, offering a new direction for recurrence quantification analysis using tools from network science [7]. Here, the challenge is to derive a distance matrix from the contact network, which can be done using graph distance. Basically three cases can be considered: (1) a plain contact network derived from a binary contact map or a recurrence plot; (2) a topology-weighted contact network; (3) a frequency-weighted contact network.

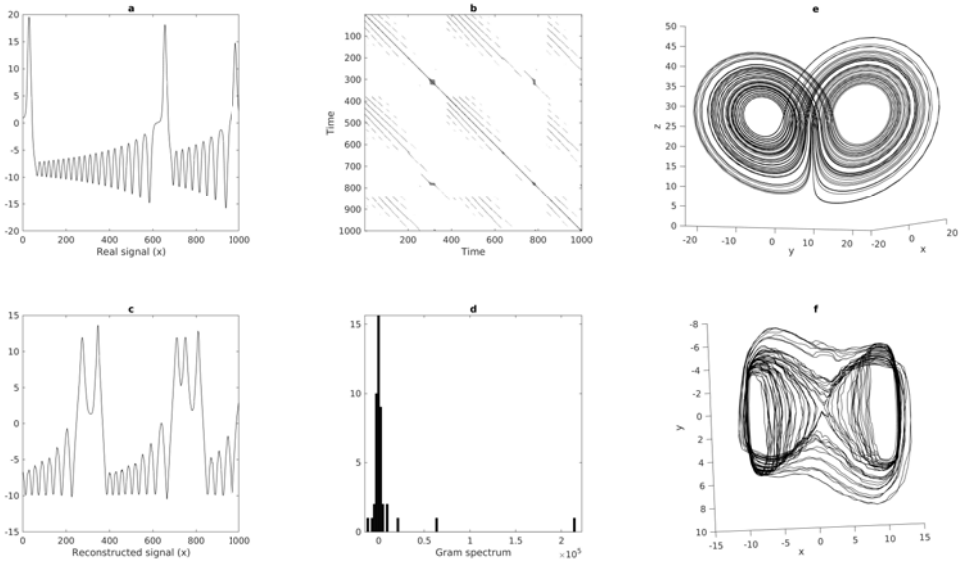


**Fig. 3. Reconstruction of Lorenz attractor from binary RP using ShRec3D.** (a) $x$-component of the simulated Lorenz dynamics ($N = 1000$ time points). (b) Corresponding binary RP, with embedding dimension $m = 8$, time delay $\tau = 3$, and dark pixels representing distances smaller than $\epsilon = 2$. (c) Principal eigenvector and (d) spectrum of the Gram matrix derived from the graph-distance matrix. Note the three markedly positive eigenvalues, consistent with an underlying spatial dimension $d = 3$. (e) Original Lorenz attractor, as in Fig. 2. (f) Attractor reconstructed by applying MDS (for a spatial dimension $d = 3$) to the graph-distance matrix (ShRec3D algorithm [16]).

### 3.1 Contact networks and graph distances

In the simplest instance, only the presence or absence of network edges is taken into account. The components of the adjacency matrix are $A_{ij} = 1$ if there is a contact between sites $i$ and $j$ (a recurrence between times $i$ and $j$), else $A_{ij} = 0$. The distance between any pair of nodes $i$ and $j$ is then defined as their graph distance, that is, the number of steps in the shortest path(s) relating them. This number can be computed using Floyd-Warshall algorithm. In the reconstruction of a trajectory or a chromosome, it is essential to add the two diagonals $(i, i+1)$ and $(i, i-1)$, i.e. to add edges (if missing) between adjacent points along time or along the linear polymer chain, respectively. This ensures the connectedness of the resulting structure, and relatedly, of the contact network, which has been shown to be a condition of reconstructibility [29]. In this case, there is no loss of information between contact maps and the underlying (dynamical or molecular) structure. The result is illustrated in Fig. 3 on the exemple of Lorenz attractor.

### 3.2 Topology-weighted contact networks

A refined procedure is to first endow the edges with a length before computing shortest-path distances. An intrinsic choice is to choose an edge length equal to 1 minus the normalized number of common neighbors [11], i.e. the Jaccard distance between the two nodes. This Jaccard distance has been shown to be equivalent to Euclidean distance in the phase space [12]. The approach is particularly well suited to single-cell Hi-C [13], where the reinforcement of the topological information compensates for the noise and sparsity of experimental data.

### 3.3 Frequency-weighted contact networks

Another procedure has been developed in an algorithm, ShRec3D, for 3D visualization of chromosomes from cell population data [16]. For such experiments, not only the presence or absence of a contact between sites $i$ and $j$, but also a continuous-valued contact frequency $f_{ij}$ is available. The length of an edge is taken to be an inverse power $1/f_{ij}^{\alpha}$ of the contact frequency. This raw length, possibly infinite if no contact has been recorded, is then replaced with the shortest-path distance. A detailed implementation of this algorithm, either in MatLab or Python, can be found in [4]. The exponent $\alpha$ can be tuned using local pairwise experiments, for instance the direct observation in a fixed cell of the spatial distance between two sites after attaching a fluorescent probe to them (FISH, fluorescence in situ hybridization), which yields $\alpha = 0.227$. Alternatively, a self-consistent criterion, based on optimizing the number of edges for which the graph distance is smaller than the raw value, has been developed [3]. It is to note that the choice of $\alpha$ depends on the objectives of the reconstruction: $\alpha = 0.2$ (in agreement with local data) ensures local accuracy, while $\alpha = 1$ ensures a consistent global shape [23]. ShRec3D achieves a fast reconstruction of the consensus chromosome structure from population Hi-C data, with tunable resolution (from megabases down to a few kilobases) and no need of implementing a polymer model of DNA. It provides a substrate for 3D genome browsers. Its application, for example to the visualization of chromosomal compartments, is illustrated in [4].

## 4 Benchmarks: Lorenz model, white noise and EEG

### 4.1 Lorenz attractor

Back to the context of dynamical systems, we compared the efficiency of the reconstruction methods on a standard benchmark, the Lorenz model [17], as done in [21] and [11]. The attractor is obtained by numerically integrating the three coupled differential equations and discarding a transient. Non linear couplings inherent to the chaotic dynamics ensure that observing only one component gives sufficient information to reconstruct the topology of the whole trajectory in the 3-dimensional phase space. According to Takens' theorem [28], the embedding dimension $m$ has to be large enough, strictly larger than twice the fractal dimension of the attractor. The reconstruction from the unthresholded RP and $m = 8$

is shown in Fig. 2, while Fig. 3 displays the results obtained using the simplest method of reconstruction (plain graph distance and MDS) applied to binary RP.

Due to the fractal structure of the Lorenz attractor, the RP is sensitive to the choice of the recurrence threshold $\epsilon$, which has to be carefully chosen, e.g. using the method developed in [22]. In contrast, our observations meet the statement done in [11] that the size $N$ does not drastically matter. As seen on Fig. 2c and Fig. 3c, the principal eigenvector of the Gram matrix already displays the most significant features of the dynamics. Another remarkable characteristic of the Gram matrix is the spectral signature of the dimension $d = 3$ of the phase space, reflecting in the presence of three markedly positive eigenvalues separated from a cluster of almost vanishing (and irrelevant) values (Fig. 2d and Fig. 3d). These two spectral characteristics of the Gram matrix are observed for both reconstruction methods, and for any large enough value of $m$ among those investigated (up to $m = 20$). As a side remark, complex (though very small) eigenvalues sometimes appear when $m$ is too small, a spurious fact already noticed in [21].

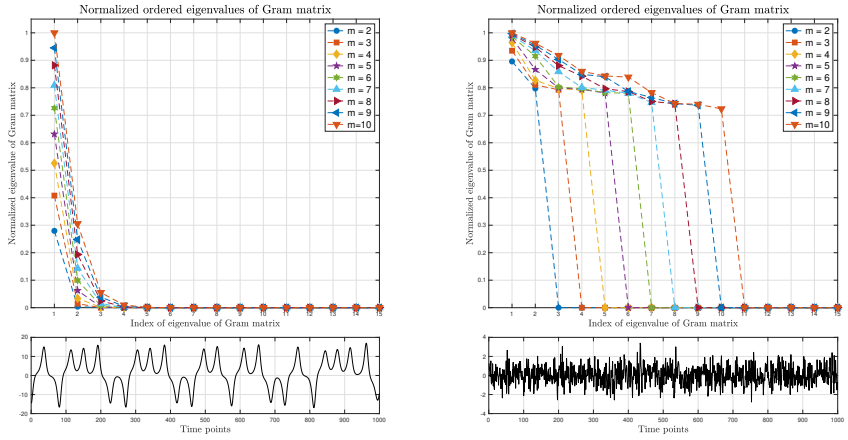


**Fig. 4. Spectral signature of space dimension: Lorenz model and white noise.** Plot of the 15 largest eigenvalues of the Gram matrix derived from the unthresholded RP, ranked in descending order along the horizontal axis, for different values of the embedding dimension $m$: (Left) starting from the $x$-component of the Lorenz attractor, see Fig. 2 and (Right) for Gaussian white noise using a time delay $\tau = 1$. The signal used ($N = 1000$ time points) is presented below each plot. For easier comparison, eigenvalues have been normalized by the largest observed one, and the values for a given dimension $m$ are connected by dashed lines as a guide for the eye.

### 4.2 White noise

We also investigated the behavior of a white noise, as it has been shown that recurrence plots are also relevant for stochastic processes [24]. We simulated $N = 1000$ independent values of a Gaussian white noise and computed the unthresholded RP. As we do not expect any remarkable feature in the reconstructed structure, we rather focused on the spectrum of the Gram matrix. A striking observation is the ever-increasing number of strictly positive Gram eigenvalues when $m$ increases. We devised a reliable counting representation by plotting the 15 largest eigenvalues, ordered in descending order, for each value of $m$. For easier comparison, the values have been normalized by the largest observed value (principal eigenvalue for $m = 10$). This analysis applied to the Lorenz model (Fig. 4, left) recovers a fixed number of three positive eigenvalues, equal to the phase space dimension $d = 3$, provided $m$ is large enough (strictly larger than 6). In contrast, the behavior observed for the white noise displays an increasing number, equal to $m$, of positive eigenvalues (Fig. 4, right). Relatedly, the 3D visualization (not shown) is highly variable and displays a gradual shift from a roughly directed motion at small values of $\tau$ and large values of $m$ to a homogenous spreading at large values of $\tau$ and $m = 3$.

### 4.3 Electroencephalographic (EEG) data

We finally benchmarked the spatial reconstruction and Gram spectrum methodology on real electroencephalographic (EEG) data available from [1]. We used a single-electrode recording, i.e. a local recording of an extended spatio-temporal dynamics, in open-eyes condition, applying a bandpass filter from 1 Hz to 40 Hz to eliminate low-frequency trend and experimental noise. We reconstructed the Gram matrix from the unthresholded RP, using a time delay $\tau = 4$ determined using either auto-correlation or AMI (average mutual information) criteria [14]. We observe that the number of positive eigenvalues of the Gram matrix increases with $m$ (Fig. 5, left) This is not unexpected as in most cases, a stochastic nature of the single-electrode EEG recording cannot be discarded using the method of surrogate data [1].We also considered the same data restricted to the $\alpha$ band (i.e. between 8 Hz and 13 Hz). As expected, the filtered data display a more regular structure. A striking observation is the lower number of positive eigenvalues in the Gram matrix (Fig. 5, right), which saturates in a way resembling the behavior observed for Lorenz attractor, although with a larger number (equal to 5). This behavior depends slightly on the electrode considered, with a number of positive eigenvalues that could reach 5 or 6 for $m = 10$.

### 4.4 Discussion: spectral signature of the spatial dimension $d$

Our study introduces a novel criterion for assessing the dimension $d$ of the phase space, i.e. the number of coupled variables involved in a dynamics generally recorded on a single observable, or the dimension of the underlying real space in the case of linear polymer chains such as proteins or chromosomes. This criterion

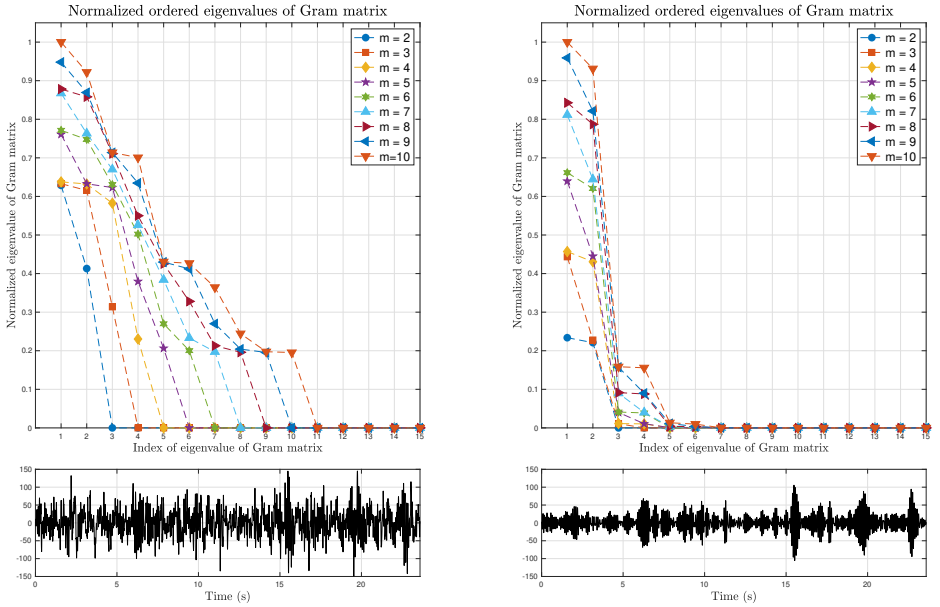


**Fig. 5. Spectral signature of space dimension: single-electrode EEG data.** Same as Fig. 4 (Left) for EEG recording from a single electrode located above the visual cortex, applying a bandpass filter from 1 Hz to 40 Hz to eliminate low-frequency trend and experimental noise; (Right) for $\alpha$-band-filtered signal. Time delay $\tau = 4$.

is based on the spectrum of the Gram matrix computed from the unthresholded RP (when available), or from the graph-distance matrix computed from the contact network. Although the Gram matrix is a $N \times N$ square matrix, we observed in the different benchmarks that it has a limited number of markedly positive eigenvalues. This number is independent of $N$ but may depend on the embedding dimension $m$. The remaining part of the spectrum consists in a cluster of eigenvalues around 0, related to observational and numerical noise. The number of positive eigenvalues saturates at $d$ for nonlinear deterministic dynamics (e.g. chaotic dynamics), provided the time delay has been properly chosen. In contrast, this number is equal to $m$ for white noise. A similar spectral behavior, with a number of positive eigenvalues increasing with $m$, is observed for the Gram matrix of a high-dimensional dynamics, e.g. a spatially extended dynamics as the brain dynamics underlying EEG data. However, the increase with $m$ may be slower than $m$ or even saturating when the dynamics displays some level of regularity, here after filtering to a limited number of periodic components ($\alpha$-band filtered single-electrode EEG signal). The extreme case is a number of eigenvalues saturating at $d$ in the case of Lorenz model capturing the three dominant modes of spatially extended atmospheric dynamics. The examples presented here

emphasize the critical choice of the embedding dimension $m$, the radius $\epsilon$ and the time delay $\tau$. How these choices affect the spectral signature would deserve a systematic exploration. These preliminaries results will prompt further research, to assess the variation with $m$ of the number of positive Gram eigenvalues and the presence of a spectral gap for different model systems. A key question is whether this dependence on $m$ of the Gram spectrum could quantitatively reflect a stochastic or high-dimensional nature of the dynamics. In the case of the spatially folded structure of a linear polymer chain, the dimension is generally known, equal to $d = 3$. The benefit of the Gram matrix spectral analysis is then to assess the strength of noise and variability, in particular when the recording of spatial contacts merges data from a sample of similar structures as in cell-population chromosome conformation capture [16].

## 5 Conclusion

We have presented an insightful analogy between recurrence plots and chromosome Hi-C maps, sharing the notion of contact map and associated contact network. We exploited this analogy to gather, within a unified methodology, several reconstructions methods from 1D series to a higher-dimensional spatial structure. This methodology demonstrates the possibility of obtaining global information about the (dynamical or molecular) structure from the local recording of contacts, i.e. the invertibility of contact maps. The reconstruction is first based on computing a graph-distance matrix from the contact network, except in the case of unthresholded RP which are already in the form of a distance matrix. The spatial structure is then obtained from the distance matrix using the toolbox of distance geometry or multidimensional scaling. This reconstruction methodology offers fast and tunable way to directly visualize the phase-space trajectory underlying a single-component time series, e.g. for comparison purposes between different conditions, or the spatially folded structure of a polymer chain. Its computational speed makes possible real-time visualization.

We introduced a related spectral signature of the dynamics, defined as the number of markedly positive eigenvalues of the Gram matrix derived from either the unthresholded RP or the graph-distance matrix. Its ability to quantitatively discriminate low-dimensional deterministic dynamics and high-dimensional or stochastic dynamics now deserves further exploration.

The analogy between RP and HiC maps also opens research directions at the crossroads between signal analysis and genomics, exploiting advances in HiC analysis for RP analysis (e.g. applying to unthresholded RP an algorithm, Boost-HiC [3], devised to enhance undersampled Hi-C maps), or conversely, exploiting recurrence quantification analysis to Hi-C maps.

## Acknowledgements

AL thanks the University of Tsukuba (Faculty of Engineering, Information and Systems) for hospitality and funding of her stay in Tsukuba, during which part

of this work has been performed. She also thanks Yoshito Hirata (University of Tsukuba) for insightful discussions, and all the organizers of the 10th International Symposium on Recurrence Plots 2023.

## References

1. Andrzejak, R. G., Lehnertz, K., Mormann, F., Rieke, C., David, P., Elger, C. E.: Indications of nonlinear deterministic and finite-dimensional structures in time series of brain electrical activity: Dependence on recording region and brain state. Physical Review E 64, 061907 (2001). doi:10.1103/PhysRevE.64.061907
2. Beals, R., Krantz, D. H., Tversky, A.: Foundations of multidimensional scaling. Psychological Review 75, 127 (1968). doi:10.1037/h0025470
3. Carron, L., Morlot, J. B., Matthys, V., Lesne, A., Mozziconacci, J.: Boost-HiC: computational enhancement of long-range contacts in chromosomal contact maps. Bioinformatics 35, 2724–2729 (2019). doi:10.1093/bioinformatics/bty1059
4. Carron, L., Morlot, J. B., Lesne, A., Mozziconacci, J.: The 3D organization of chromatin colors in mammalian nuclei. Methods Mol. Biol. 2301, 317–336 (2022). doi:10.1007/978-1-0716-1390-0_17
5. Dekker, J., Rippe K., Dekker, M. Kleckner, N.: Capturing chromosome conformation, Science 295, 1306–1311 2002. doi:10.1126/science.1067799
6. Di Paola, L., De Ruvo, M., Paci, P., Santoni, D., Giuliani, A.: Protein contact networks: an emerging paradigm in chemistry. Chemical Reviews 113, 1598–1613 (2013). doi:10.1021/cr3002356
7. Donner, R. V., Zou, Y., Donges, J. F., Marwan, N., Kurths, J.: Recurrence networks. A novel paradigm for nonlinear time series analysis. New Journal of Physics 12, 033025 (2010). doi:10.1088/1367-2630/12/3/033025
8. Eckmann, J. P., Kamphorst, S. O., Ruelle, D.: Recurrence plots of dynamical systems. Europhysics Letters 4, 973–977 (1987). doi:10.1209/0295-5075/4/9/004
9. Faure, P., Lesne, A.: Recurrence plots for symbolic sequences. International Journal of Bifurcation and Chaos 20, 1731–1749 (2010). doi:10.1142/S0218127410026794
10. Havel, T. F., Kuntz, I. D., Crippen, G. M.: The theory and practice of distance geometry. Bulletin of Mathematical Biology 45, 665–720 (1983). doi:10.1007/BF02460044
11. Hirata, Y., Horai, S., Aihara, K.: Reproduction of distance matrices and original time series from recurrence plots and their applications. The European Physical Journal Special Topics 164, 13–22 (2008). doi:https://doi.org/10.1140/epjst/e2008-00830-8
12. Hirata, Y., Komuro, M., Horai, S., Aihara, K.: Faithfulness of recurrence plots: a mathematical proof. International Journal of Bifurcation and Chaos 25, 1550168 (2015). doi:10.1142/S0218127415501680
13. Hirata, Y., Oda, A., Ohta, K., Aihara, K.:Three-dimensional reconstruction of single-cell chromosome structure using recurrence plots. Scientific Reports 6, 34982 (2016). doi:10.1140/epjst/e2008-00830-8
14. Kantz, H., Schreiber, T.: Nonlinear time series analysis. Cambridge University Press (2004). doi:10.1017/CBO9780511755798
15. Kenkel, N. C., Orlóci, L.: Applying metric and nonmetric multidimensional scaling to ecological studies: some new results. Ecology 67, 919-928 (1986). doi:10.2307/1939814

16. Lesne, A., Riposo, J.,Roger, P. ,Cournac, A., Mozziconacci, J.: 3D genome reconstruction from chromosomal contacts. Nature Methods 11, 1141–1143 (2014). doi:10.1038/nmeth.3104
17. Lorenz, E. N.: Deterministic nonperiodic flow. Journal of Atmospheric Sciences 20, 130-1-41 (1963). doi:10.1175/1520-0469(1963)020⟨0130:DNF⟩2.0.CO;2
18. http://www.recurrence-plot.tk/programmes.php
19. Marwan, N., Romano, M. C., Thiel, M., Kurths, J.: Recurrence plots for the analysis of complex systems, Physics Reports 438, 237–329 (2007). doi:10.1016/j.physrep.2006.11.001
20. Marwan, N., Kraemer, K. H.: Trends in recurrence analysis of dynamical systems. The European Physical Journal Special Topics 232, 5–27 (2023). doi:10.1140/epjs/s11734-022-00739-8
21. McGuire, G., Azar, N. B., Shelhamer, M.: Recurrence matrices and the preservation of dynamical properties. Physics Letters A 237, 43–47 (1997). doi:10.1016/S0375-9601(97)00697-X
22. Medrano, J., Kheddar, A., Lesne, A., Ramdani, S.: Radius selection using kernel density estimation for the computation of nonlinear measures. Chaos: An Interdisciplinary Journal of Nonlinear Science 31, 083131 (2021). doi:10.1063/5.0055797
23. Morlot, J. B., Mozziconacci, J., Lesne, A.: Network concepts for analyzing 3D genome structure from chromosomal contact maps. EPJ Nonlinear Biomedical Physics 4, 1–15 (2016). doi:10.1140/epjnbp/s40366-016-0029-5
24. Ramdani, S., Bouchara, F., Lagarde, J., Lesne, A.: Recurrence plots of discrete-time gaussian stochastic processes. Physica D: Nonlinear Phenomena 330, 17-31 (2016). doi:10.1063/1.5030522
25. Rao, S. S., Huntley, M. H., Durand, N. C., Stamenova, et al.: A 3D map of the human genome at kilobase resolution reveals principles of chromatin looping. Cell 159, 1665–1680 (2014). doi:10.1016/j.cell.2014.11.021
26. Sipers, A., Borm, P., Peeters, R.: On the unique reconstruction of a signal from its unthresholded recurrence plot. Physics Letters A 375, 2309–2321 (2011). doi:10.1016/j.physleta.2011.04.040
27. Sneath, P. H. A.: Distortions of taxonomic structure from incomplete data on a restricted set of reference strains. Microbiology 129, 1045-1073 (1983). doi:10.1099/00221287-129-4-1045
28. Takens, F.: Detecting Strange Attractors in Turbulence. In: Rand, D.A. and Young, L.-S. (eds.) Dynamical Systems and Turbulence, pp. 366–381. Springer, Heidelberg (1981). doi:10.1007/BFb0091924
29. Thiel, M., Romano, M. C., Kurths, J.: How much information is contained in a recurrence plot? Physics Letters A 330, 343–349 (2004). doi:10.1016/j.physleta.2004.07.050
30. Webber Jr, C. L., Giuliani, A., Zbilut, J. P., Colosimo, A.: Elucidating protein secondary structures using alpha-carbon recurrence quantifications. Proteins: Structure, Function, and Bioinformatics 44, 292–303 (2001). doi:10.1002/prot.1094
31. Webber, C. L., Marwan, N. Recurrence quantification analysis. Theory and best practices, Springer (2015). doi:10.1007/978-3-319-07155-8